

---

## **Steady-state cornering equilibria and stabilisation for a vehicle during extreme operating conditions**

---

**Efstathios Velenis\***

School of Engineering and Design,  
Brunel University,  
Uxbridge, Middlesex, UB8-3PH, UK  
E-mail: [efstathios.velenis@brunel.ac.uk](mailto:efstathios.velenis@brunel.ac.uk)  
\*Corresponding author

**Emilio Frazzoli**

Department of Aeronautics and Astronautics,  
Massachusetts Institute of Technology,  
Cambridge, MA 02139, USA  
E-mail: [frazzoli@mit.edu](mailto:frazzoli@mit.edu)

**Panagiotis Tsiotras**

Daniel Guggenheim School of Aerospace Engineering,  
Georgia Institute of Technology,  
Atlanta, GA 30332-0150, USA  
E-mail: [tsiotras@gatech.edu](mailto:tsiotras@gatech.edu)

**Abstract:** In this work we study steady-state cornering conditions for a single-track vehicle model, without imposing restrictive conditions on the tyre slip. Inspired by recent progress in the understanding of advanced driving techniques, we design a sliding-mode control scheme stabilising steady-state cornering conditions, using only longitudinal control inputs, i.e., accelerating/braking torques applied at the front and/or rear wheels. The effectiveness of the control scheme is demonstrated in a variety of simulation scenarios, motivated by competitive race driving. Results are presented using both the baseline model, and an increased-fidelity model taking into account suspension dynamics.

**Keywords:** vehicle dynamics; technical driving; drift; steady-state cornering; nonlinear tyre characteristics; stabilisation; sliding mode control.

**Reference** to this paper should be made as follows: Velenis, E., Frazzoli, E. and Tsiotras, P. (2010) 'Steady-state cornering equilibria and stabilisation for a vehicle during extreme operating conditions', *Int. J. Vehicle Autonomous Systems*, Vol. 8, Nos. 2/3, pp.217–241.

**Biographical notes:** Efstathios Velenis joined the Faculty of the School of Engineering and Design at Brunel University in 2008 as a Lecturer. Prior to joining Brunel University he held a Post-Doctoral Fellow position at Georgia Institute of Technology and Ford Motor Company.

He received his MSc and PhD degrees in Aerospace Engineering from Georgia Institute of Technology in 2000 and 2006 respectively and his Engineering Diploma in Mechanical Engineering from the National Technical University of Athens in 1999. His current research interests include vehicle dynamics and control, modelling of expert driving techniques, active safety systems for passenger vehicles and high-speed control of autonomous vehicles.

Emilio Frazzoli is an Associate Professor of Aeronautics and Astronautics with the Laboratory for Information and Decision Systems at the Massachusetts Institute of Technology. He received a Laurea Degree in Aerospace Engineering from the University of Rome, 'La Sapienza', in 1994, and a PhD in Navigation and Control Systems from the Massachusetts Institute of Technology, in 2001. Between 2001 and 2006 he was on the faculty of the University of Illinois, Urbana Champaign, and of the University of California, Los Angeles. He is an Associate Fellow of the AIAA and a Senior Member of the IEEE, and is currently an Associate Editor for the AIAA J. of Guidance, Control, and Dynamics. He was the recipient of a NSF CAREER award. His main research interests lie in the general area of planning and control for mobile cyber-physical systems, with a particular emphasis on autonomous vehicles, mobile robotics, and transportation networks.

Panagiotis Tsiotras is a Professor in the School of Aerospace Engineering at the Georgia Institute of Technology. From 1994–1998 he was with the Department of Mechanical and Aerospace Engineering at the University of Virginia. He has also held visiting appointments with INRIA, Rocquencourt, the Laboratoire d'Automatique de Grenoble, and the Ecole des Mines de Paris in France. His research interests are in dynamics and nonlinear and optimal control of aerospace, automotive and mechanical systems, and vehicle autonomy. He is a recipient of the NSF CAREER award, the Sigma Xi President and Visitor's Award for Excellence in Research as well as numerous fellowships and scholarships. He is an Associate Editor for the *IEEE Transaction of Automatic Control* and the *IEEE Control Systems Magazine*, and a past Associate Editor of the *AIAA Journal of Guidance, Control, and Dynamics* and of the *International Journal Dynamics and Control*. He is a Fellow of the AIAA, and a Senior Member of the IEEE.

---

## 1 Introduction

The introduction of vehicle stability systems has had a significant impact on passenger vehicle safety. Several statistics show that these systems have considerably reduced road traffic accidents (Dang, 2004). There is a variety of results in the literature towards enhancing the performance of passenger vehicle stability systems. Stability control is usually implemented via differential braking (independent braking control on all four wheels) (van Zanten et al., 2000), active steering (Ackermann, 1997; Yoshimoto et al., 1999), active-differential (Ikushima and Sawase, 1995; Piyabongkarn et al., 2007) and, more recently, via integrated chassis

control (Hac and Bodie, 2002; Trachtler, 2004; Wei et al., 2006). The latter incorporate and coordinate active chassis systems including differential braking, traction control, active steering and active suspension systems. Alternative means of power transmission for electric and hybrid vehicles have also allowed the development of vehicle stability systems based on independent wheel torque control (Tahami et al., 2003; Kim et al., 2008). The common objective of all of the above systems is to restrict the operation of the vehicle, such that the tyres operate within the linear region of the wheel slip-tyre friction characteristic, and to match the vehicle's response to one of a simple vehicle model in steady-state cornering (Gillespie, 1992). In this way, the average driver can maintain control of the vehicle during an emergency. It is worth pointing out that, while traditionally stability analysis and control considered solely the lateral dynamics of the vehicle, there have been recent results incorporating longitudinal and lateral dynamics and the coupling of tyre forces in the longitudinal/lateral directions (Wei et al., 2006; Yi and Tseng, 2009).

Accident avoidance during an emergency may require taking advantage of the full handling capacity of the vehicle, and the employment of expert driving skills, rather than restricting the response of the vehicle. It is envisioned that a new generation of active safety systems will take advantage of the increased situational awareness of modern and future vehicles, as demonstrated during the 2005 DARPA Grand Challenge and the 2007 DARPA Urban Challenge autonomous vehicle competitions, and use expert driver techniques to actively manoeuvre vehicles away from accidents. With this vision in mind, a mathematical analysis of expert driving techniques was initiated in Velenis et al. (2007a, 2007b, 2008a, 2008b). The driving techniques investigated in these references were those used by rally drivers, which clearly involve operation of the vehicle outside the stable operation envelope enforced by the current stability systems. Data collected during execution of different rally driving techniques by an expert driver in Velenis et al. (2007b, 2008a) show operation of the vehicle at high sideslip angles, suggesting that the tyres operate well inside the nonlinear region. These expert driving techniques were reproduced using nonlinear programming optimisation Velenis et al. (2007a, 2007b, 2008a, 2008b). It was shown that cornering at high sideslip angles may be necessary for time-optimal cornering with limited preview of the road. Furthermore, expert drivers' empirical guidelines on controlling the vehicle under such extreme operating conditions, via throttle/brake control and longitudinal load transfer, were validated. The analysis in Velenis et al. (2007a, 2007b, 2008a, 2008b) provided a significant understanding of the dominant effects during execution of expert driving techniques, but the open-loop approach of the optimisation is not implementable in the presence of uncertainties.

A study of the stability of vehicle cornering equilibria with the tyres operating at their full range (including linear and nonlinear range) and the design of a stabilising front wheel steering controller appear in Ono et al. (1998). The authors of this work used a single-track vehicle model and assumed pure cornering conditions, that is, absence of longitudinal forces (tractive or braking) at the wheels. A phase-plane analysis of the cornering equilibria in this work was followed by the design of a linear robust stabilising steering controller. The stability analysis of cornering equilibria considering nonlinear tyre characteristics and using phase-plane techniques is also discussed in Yi and Tseng (2009). In the latter

a combined motion tyre friction model is used to characterise the coupling of tyre forces in the longitudinal and lateral directions. High sideslip angle (drifting) steady-state cornering conditions were examined in Abdulrahim (2006) using the lateral dynamics of a four wheel vehicle model, neglecting the equilibrium of forces in the longitudinal direction. A combined traction/cornering tyre friction model was incorporated and under the assumption of Rear-Wheel-Drive (RWD) transmission the steady-state steering angle and rear wheel slip ratio were derived for a given pair of steady-state sideslip angle and yaw rate. Steady-state drifting or power-slide using a four wheel vehicle model with RWD transmission, incorporating longitudinal and lateral dynamics, load transfer effects and a combined motion tyre friction model, have been discussed in Edelmann et al. (2008). The set of steady-state equations were solved numerically and stability of the equilibria was studied using a root locus method. A simple single-track model of an RWD vehicle incorporating longitudinal and lateral vehicle dynamics and a simplified combined motion tyre friction model were used in Hindiyeh and Gerdes (2009) for a stability analysis and classification of cornering equilibria including drifting conditions. Using a simplified tyre friction model the authors in Hindiyeh and Gerdes (2009) neglected the wheel speed dynamics and considered the rear wheel longitudinal force as a control input. Neglecting load transfer effects and wheel rotational dynamics, the vehicle model in Hindiyeh and Gerdes (2009) is of low order and more suitable for control design compared, for instance, to the high fidelity model of Edelmann et al. (2008).

The existence of steady-state cornering conditions with excessive vehicle sideslip was also demonstrated in Frazzoli (2008). In this reference the author derived explicit steady-state cornering conditions for a single-track vehicle model using a wheel slip based combined motion tyre friction model, and considering longitudinal load transfer effects, which play a key role in the execution of expert driving techniques as discussed in Velenis et al. (2007a, 2007b, 2008a, 2008b). The simplifying assumption of a free rolling rear wheel in Frazzoli (2008), which suggests a front-wheel-drive configuration, allowed for considerable decoupling of the steady-state equations and efficient calculation of the equilibria. Building on the approach of Frazzoli (2008), in this work we allow for the combined cornering and traction/braking forces to develop on both front and rear tyres, assuming independent front and rear longitudinal slip inputs, and derive cornering equilibria achievable by different transmission configurations (front-, rear-, all-wheel-drive). The vehicle model is enriched with wheel speed dynamics and load transfer effects, which results in a higher order model than the one in Hindiyeh and Gerdes (2009), remaining, however, suitable for control design. In particular, we design a control scheme using independent wheel front and rear torque inputs to stabilise the vehicle with respect to steady-states cornering conditions including drifting. In the proposed control scheme the steering angle is fixed at its steady-state value, and stabilisation is achieved purely by regulation of tractive/braking forces in analogy to previously studied expert driving techniques Velenis et al. (2007a, 2007b, 2008a, 2008b). We envision the ability to control the vehicle in a wide range of steady-state cornering conditions, including large vehicle sideslip angles, as an enabling technology towards the development of full-envelope vehicle control technologies, emulating the skills of expert drivers, e.g., for accident avoidance or high-performance driving. For example, a library of motion primitives consisting of a collection of pre-computed steady-state trajectories and controlled transitions can be used to construct 'aggressive' trajectories on the fly (Frazzoli et al., 2002, 2005).

In the following, we first introduce a single-track model with nonlinear tyre characteristics, taking into consideration the normal load transfer from front to rear wheels during forward acceleration. Steady-state cornering is defined as cornering along a path of constant curvature, with constant speed and sideslip angle. For a given triplet of corner curvature, vehicle speed and sideslip angle, we calculate the necessary front and rear wheel longitudinal slip quantities (slip ratios), and front wheel steering angle, necessary to maintain the steady-state cornering condition. Steady-state wheel speeds and the corresponding torques at the front and the rear axles are then calculated using the associated wheel speed dynamics. A control scheme is presented, consisting of a linear quadratic regulator, which produces the necessary front and rear longitudinal slip quantities to stabilise the vehicle to the desired triplet of steady-state speed, sideslip angle and yaw rate, and a sliding-mode controller, which uses front and rear wheel torques to drive the front and rear longitudinal slips to the values dictated by the LQR. A vehicle model of increased fidelity, namely a single-track model with suspension dynamics, is used to demonstrate the efficiency of the controller.

## 2 Vehicle model

In this section we introduce a single-track vehicle model with nonlinear tyre characteristics. We employ a static map to calculate the normal load transfer from front to rear wheels, and vice-versa, arising from the longitudinal acceleration of the vehicle. This model maintains a satisfactory level of fidelity for reproducing the dominant vehicle dynamic effects during extreme operating conditions, such as those encountered in rally driving (Velenis et al., 2007a, 2008a, 2008b).

### 2.1 Equations of motion of the single-track model

The equations of motion of the single-track model (Figure 1) may be expressed in a body-fixed frame with the origin at the vehicle's Centre of Gravity (CG) as follows:

$$m(\dot{V}_x - V_y \dot{\psi}) = f_{Fx} \cos \delta - f_{Fy} \sin \delta + f_{Rx} \quad (1)$$

$$m(\dot{V}_y + V_x \dot{\psi}) = f_{Fx} \sin \delta + f_{Fy} \cos \delta + f_{Ry} \quad (2)$$

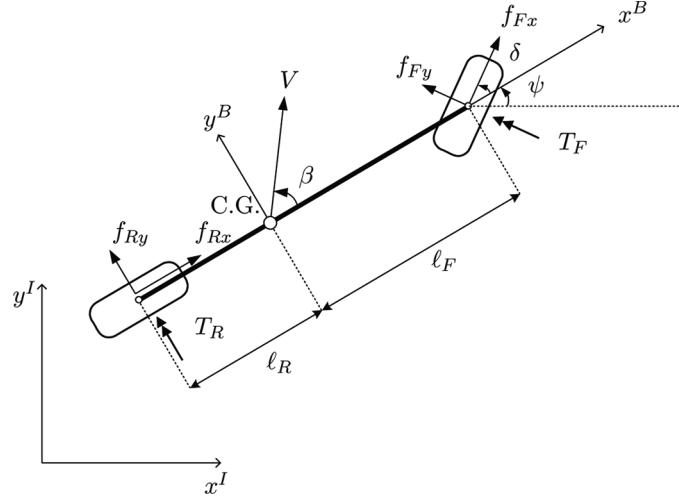
$$I_z \ddot{\psi} = (f_{Fy} \cos \delta + f_{Fx} \sin \delta) \ell_F - f_{Ry} \ell_R, \quad (3)$$

where

$$V_x = V \cos \beta, \quad V_y = V \sin \beta.$$

In the above equations  $m$  is the vehicle's mass,  $I_z$  is the moment of inertia of the vehicle about the vertical axis,  $V_x$  and  $V_y$  are the body-frame components of the vehicle velocity  $V$ ,  $\psi$  is the yaw angle of the vehicle, and  $\delta$  is the steering angle of the front wheel. By  $f_{ij}$  ( $i = F, R$  and  $j = x, y$ ) we denote the longitudinal and lateral friction forces at the front and rear wheels, respectively.

**Figure 1** Single-track vehicle model



The vehicle slip angle is given by

$$\beta = \text{atan}\left(\frac{\dot{y}}{\dot{x}}\right) - \psi = \text{atan}\left(\frac{V_y}{V_x}\right)$$

where  $\dot{x}$  and  $\dot{y}$  are the inertial frame components of the vehicle speed.

### 2.2 Tyre forces

By tyre slip we refer to the non-dimensional relative velocity of the tyre with respect to the road. In Bakker et al. (1987) the practical tyre slip quantities, namely the practical longitudinal slip  $\kappa_i$  and the slip angle  $\alpha_i$  ( $i = F, R$ ), are defined as follows:

$$\kappa_i = \frac{\omega_i r_i - V_{ix}}{V_{ix}}, \quad \tan \alpha_i = \frac{V_{iy}}{V_{ix}},$$

where the index  $i = F, R$  denotes the front and rear axle of the single-track model respectively,  $\omega_i$  is the angular rate of the wheel,  $r_i$  is the wheel radius, and  $V_{ij}$ , ( $i = F, R, j = x, y$ ) are the tyre frame components of the vehicle velocity vector at the front and rear wheels.

The theoretical slip quantities (Bakker et al., 1987) are defined as:

$$s_{ix} = \frac{V_{ix} - \omega_i r_i}{\omega_i r_i} = -\frac{\kappa_i}{1 + \kappa_i}, \quad s_{iy} = \frac{V_{iy}}{\omega_i r_i} = \frac{\tan \alpha_i}{1 + \kappa_i}. \quad (4)$$

We notice that

$$s_{iy} = (1 + s_{ix}) \tan \alpha_i.$$

The overall, or total, slip at each tyre is defined by

$$s_i = \sqrt{s_{ix}^2 + s_{iy}^2}.$$

The vehicle velocity components at the front and rear wheels of the single-track model along each wheel's longitudinal and lateral axes are given by:

$$\begin{aligned} V_{Fx} &= V \cos(\beta - \delta) + \dot{\psi} \ell_f \sin \delta, & V_{Fy} &= V \sin(\beta - \delta) + \dot{\psi} \ell_f \cos \delta, \\ V_{Rx} &= V \cos(\beta), & V_{Ry} &= V \sin(\beta) - \dot{\psi} \ell_R. \end{aligned}$$

Assuming linear dependence of the tyre friction forces on the tyre normal force we obtain

$$\mu_i = f_i / f_{iz}, \quad \mu_{ij} = f_{ij} / f_{iz}, \quad i = F, R, \quad j = x, y, \quad (5)$$

where  $f_i = \sqrt{f_{ix}^2 + f_{iy}^2}$  is the total friction force at each tyre,  $\mu_i$  is the total friction coefficient at each tyre,  $\mu_{ij}$  are the longitudinal and lateral friction coefficients at each tyre, and  $f_{iz}$  are the normal loads at the front and rear tyres.

We calculate the total friction coefficient using Pacejka's 'magic formula' (MF) (Bakker et al., 1987) as follows:

$$\mu_i(s_i) = \text{MF}(s_i) = D \sin(\text{Catan}(Bs_i)).$$

Assuming symmetric tyre characteristics with respect to the longitudinal and lateral directions, the total friction force for each tyre lies within the so-called friction circle. In this case, the longitudinal and lateral tyre friction components are given by:

$$\mu_{ij} = -\frac{s_{ij}}{s_i} \mu(s_i). \quad (6)$$

Neglecting suspension dynamics, the equilibrium of forces in the vertical direction and the equilibrium of moments about the body- $y$  axis are used to find front and rear axle normal loads:

$$0 = f_{Fz} + f_{Rz} - mg, \quad (7)$$

$$0 = h(f_{Fx} \cos \delta - f_{Fy} \sin \delta + f_{Rx}) + f_{Fz} \ell_F - f_{Rz} \ell_R, \quad (8)$$

where  $h$  is the height of the CG from the road surface. Assuming linear dependence of the tyre friction forces on the tyre normal load (5), equations (7) and (8) result in the following expressions for the front and rear wheel normal loads:

$$f_{Fz} = \frac{\ell_R mg - h mg \mu_{Rx}}{L + h(\mu_{Fx} \cos \delta - \mu_{Fy} \sin \delta - \mu_{Rx})}, \quad (9)$$

$$f_{Rz} = mg - f_{Fz}. \quad (10)$$

### 3 Steady-state cornering conditions

In this section we derive steady-state cornering conditions for the vehicle model of the previous section. For a given corner curvature, vehicle speed and sideslip angle, we calculate the corresponding tyre friction forces of the front and rear wheels.

Steady-state cornering is characterised by a trajectory of constant radius  $R$ , negotiated at a constant speed  $V$ , and constant yaw rate and slip angle:

$$R = R^{\text{ss}} = \text{const.}, \quad V = V^{\text{ss}} = \text{const.}, \quad \dot{\psi} = \dot{\psi}^{\text{ss}} = \frac{V^{\text{ss}}}{R^{\text{ss}}}, \quad \beta = \beta^{\text{ss}} = \text{const.}$$

Under steady-state cornering conditions, equations (1)–(3), (7) and (8) are summarised below:

$$-\frac{m(V^{\text{ss}})^2}{R^{\text{ss}}} \sin \beta^{\text{ss}} = f_{Fx}^{\text{ss}} \cos \delta^{\text{ss}} - f_{Fy}^{\text{ss}} \sin \delta^{\text{ss}} + f_{Rx}^{\text{ss}}, \quad (11)$$

$$\frac{m(V^{\text{ss}})^2}{R^{\text{ss}}} \cos \beta^{\text{ss}} = f_{Fx}^{\text{ss}} \sin \delta^{\text{ss}} + f_{Fy}^{\text{ss}} \cos \delta^{\text{ss}} + f_{Ry}^{\text{ss}}, \quad (12)$$

$$0 = (f_{Fx}^{\text{ss}} \sin \delta^{\text{ss}} + f_{Fy}^{\text{ss}} \cos \delta^{\text{ss}}) \ell_F - f_{Ry}^{\text{ss}} \ell_R, \quad (13)$$

$$0 = f_{Fz}^{\text{ss}} + f_{Rz}^{\text{ss}} - mg, \quad (14)$$

$$0 = h (f_{Fx}^{\text{ss}} \cos \delta^{\text{ss}} - f_{Fy}^{\text{ss}} \sin \delta^{\text{ss}} + f_{Rx}^{\text{ss}}) + f_{Fz}^{\text{ss}} \ell_F - f_{Rz}^{\text{ss}} \ell_R. \quad (15)$$

In the following, we derive the conditions that the rear and front wheel slip quantities  $s_{ij}$  ( $i = F, R, j = x, y$ ) and corresponding wheel forces  $f_{ij}$  need to satisfy in order for the vehicle to maintain a steady-state triplet  $(R^{\text{ss}}, V^{\text{ss}}, \beta^{\text{ss}})$ . Constraints with regards to the vehicle's transmission type (front-, rear- or all-wheel-drive) are neglected for the time being to simplify the calculations, and we allow for both tractive and braking forces to develop on both front and rear wheels assuming independently driven wheels, as in Kim et al. (2008).

### 3.1 Rear axle steady-state equations

Equations (12) and (13) can be solved for  $f_{Ry}$  as a function of  $V^{\text{ss}}$ ,  $R^{\text{ss}}$  and  $\beta^{\text{ss}}$ , resulting in

$$f_{Ry}^{\text{ss}} = \frac{m(V^{\text{ss}})^2}{R^{\text{ss}}} \cos \beta^{\text{ss}} \frac{\ell_F}{\ell_F + \ell_R}.$$

Equations (11), (14) and (15) lead to the following expressions for the front and rear axle normal loads as functions of  $V^{\text{ss}}$ ,  $R^{\text{ss}}$  and  $\beta^{\text{ss}}$ :

$$f_{Rz}^{\text{ss}} = \frac{mg\ell_F - mh(V^{\text{ss}})^2 \sin \beta^{\text{ss}}/R^{\text{ss}}}{\ell_F + \ell_R}, \quad (16)$$

$$f_{Fz}^{\text{ss}} = \frac{mg\ell_R + mh(V^{\text{ss}})^2 \sin \beta^{\text{ss}}/R^{\text{ss}}}{\ell_F + \ell_R}. \quad (17)$$

Hence, given  $V^{\text{ss}}$ ,  $R^{\text{ss}}$  and  $\beta^{\text{ss}}$  we can compute the steady-state  $\mu_{Ry}^{\text{ss}}$  from

$$\mu_{Ry}^{\text{ss}} = \frac{f_{Ry}^{\text{ss}}}{f_{Rz}^{\text{ss}}},$$

as well as  $\tan(\alpha_R^{\text{ss}})$ , from

$$\tan(\alpha_R^{\text{ss}}) = \frac{V^{\text{ss}} \sin \beta^{\text{ss}} - V^{\text{ss}} \ell_R/R^{\text{ss}}}{V^{\text{ss}} \cos \beta^{\text{ss}}}.$$

Pacejka's magic formula and the slip definitions result in the following three equations with three unknowns, namely  $s_R^{ss}$ ,  $s_{Rx}^{ss}$  and  $s_{Ry}^{ss}$ :

$$\tan(\alpha_R^{ss}) = \frac{s_{Ry}^{ss}}{1 + s_{Rx}^{ss}}, \quad (18)$$

$$s_R^{ss} = \sqrt{(s_{Rx}^{ss})^2 + (s_{Ry}^{ss})^2}, \quad (19)$$

$$\mu_{Ry}^{ss} = -\frac{s_{Ry}^{ss}}{s_R^{ss}} \text{MF}(s_R^{ss}). \quad (20)$$

Solving equations (18)–(20) for the rear tyre slip quantities, finally leads to the computation of the longitudinal friction force at the rear wheel:

$$\mu_R^{ss} = \text{MF}(s_R^{ss}), \quad \mu_{Rx}^{ss} = -\frac{s_{Rx}^{ss}}{s_R^{ss}} \mu_R^{ss}, \quad f_{Rx}^{ss} = \mu_{Rx}^{ss} f_{Rz}^{ss}.$$

### 3.2 Front axle steady-state equations

Equations (11) and (12) result in the following calculation of the total front axle friction force, as a function of the rear axle forces and the steady-state triplet ( $R^{ss}$ ,  $V^{ss}$ ,  $\beta^{ss}$ ):

$$\begin{aligned} f_F^{ss} &= \sqrt{(f_{Fx}^{ss})^2 + (f_{Fy}^{ss})^2} \\ &= \sqrt{\frac{m^2 (V^{ss})^4}{(R^{ss})^2} + (f_{Rx}^{ss})^2 + (f_{Ry}^{ss})^2 + 2 \frac{m (V^{ss})^2}{R^{ss}} (f_{Rx}^{ss} \sin \beta^{ss} - f_{Ry}^{ss} \cos \beta^{ss})}. \end{aligned}$$

Given the front axle normal load from equation (16), we also get

$$\mu_F^{ss} = \frac{f_F^{ss}}{f_{Fz}^{ss}}, \quad s_F^{ss} = \text{MF}^{-1}(\mu_F^{ss}) = \tan(\text{asin}(\mu_F^{ss}/D)/C)/B.$$

Applying the friction circle equation (6) and the friction coefficient definition (5) at the front axle forces in equation (11) results in:

$$\frac{m (V^{ss})^2}{R^{ss}} \sin \beta^{ss} = \frac{f_F^{ss}}{s_F^{ss}} (s_{Fx}^{ss} \cos \delta^{ss} - s_{Fy}^{ss} \sin \delta^{ss}) - f_{Rx}^{ss}. \quad (21)$$

Recalling the definitions of front lateral slip and total front slip

$$\frac{s_{Fy}^{ss}}{1 + s_{Fx}^{ss}} = \frac{V^{ss} \sin(\beta^{ss} - \delta^{ss}) + V^{ss} \ell_F \cos \delta^{ss} / R^{ss}}{V^{ss} \cos(\beta^{ss} - \delta^{ss}) + V^{ss} \ell_F \sin \delta^{ss} / R^{ss}} \quad (22)$$

$$s_F^{ss} = \sqrt{(s_{Fx}^{ss})^2 + (s_{Fy}^{ss})^2}. \quad (23)$$

and solving equations (21)–(23) for the front tyre slip quantities and steering angle, leads finally to the computation of the longitudinal and lateral friction forces at the front wheel:

$$f_{Fj}^{ss} = -\frac{s_{Fj}^{ss}}{s_F^{ss}} \text{MF}(s_F^{ss}) f_{Fz}^{ss}, \quad j = x, y.$$

### 3.3 Steady-state wheel speeds and torque inputs

In Sections 3.1 and 3.2 we calculated the front and rear tyre forces  $f_{ij}^{ss}$ , ( $i = F, R$ ,  $j = x, y, z$ ), the associated tyre slip quantities  $s_{ij}^{ss}$ , ( $i = F, R, j = x, y$ ) and the front wheel steering angle  $\delta^{ss}$  required to maintain a steady-state triplet  $(R^{ss}, V^{ss}, \beta^{ss})$ . Next, we calculate the steady-state wheel speeds  $\omega_i^{ss}$ , ( $i = F, R$ ) and input wheel torques  $T_i^{ss}$ , ( $i = F, R$ ).

From the definition of the longitudinal wheel slip we find:

$$\omega_F = \frac{V_{Fx}}{(1 + s_{Fx})r} = \frac{V \cos(\beta - \delta) + \dot{\psi} \ell_F \sin \delta}{(1 + s_{Fx})r}, \quad (24)$$

$$\omega_R = \frac{V_{Rx}}{(1 + s_{Rx})r} = \frac{V \cos \beta}{(1 + s_{Rx})r}. \quad (25)$$

Neglecting rolling resistances at the front and rear tyres, the equation describing the rotation of the wheels is as follows:

$$I_{wi} \dot{\omega}_i = T_i - f_{ix} r_i, \quad i = F, R, \quad (26)$$

where  $I_{wi}$  ( $i = F, R$ ) is the moment of inertia of each wheel about its axis of rotation,  $r_i$  ( $i = F, R$ ) is the radius of each wheel and  $T_i$  is the driving/braking torque applied at each wheel. In steady-state motion the wheel speeds maintain constant values as in equations (24) and (25), thus equation (26) can be used to calculate the steady-state torques at each wheel:

$$T_i^{ss} = f_{ix}^{ss} r_i, \quad i = F, R.$$

### 3.4 Steady-state conditions: numerical examples

In this section we present several cases of steady-state cornering under the assumption of independent front and rear wheel torque control. For a given steady-state triplet  $(R^{ss}, V^{ss}, \beta^{ss})$ , we seek for the steady-state slip quantities, steering angle and tyre friction forces at the front and rear tyres using the derivations of Sections 3.1 and 3.2. In addition, we calculate the steady-state wheel speeds and torque inputs using the derivations of Section 3.3, as well as the front and rear wheel slip angle  $\alpha_i^{ss} = \tan^{-1}(V_{iy}^{ss}/V_{ix}^{ss})$ ,  $i = F, R$ . The parameters of the vehicle used for the calculations are given in Table 1.

In Table 2 we present a number of steady-state conditions including the values of steady-state steering angle, front and rear wheel torques, angular rates and slip angles. We observe that multiple steady-states corresponding to the same path radius and vehicle speed are possible, as revealed by Cases (a) and (b), (k) and (n), (l) and (o), (m) and (p) in Table 2. At this stage we have assumed independent torque inputs for front and rear wheels. If we were to consider more traditional types of transmission, such as front-, rear-, and all-wheel-drive (FWD, RWD and AWD) we would need to classify these steady-states according to their feasibility with respect to a specific type of transmission. For instance, we notice that for the steady-state conditions (d), (g) and (j) the input torques satisfy  $T_F^{ss} > 0$  and  $T_R^{ss} > 0$ , which are not achievable by a FWD or a RWD vehicle. The above

**Table 1** Vehicle parameters

Parameter	Value
$m$ (kg)	1450
$I_z$ (kg m <sup>2</sup> )	2741.9
$\ell_F$ (m)	1.1
$\ell_R$ (m)	1.59
$h$ (m)	0.4
$I_{wF}, I_{wR}$ (kgm <sup>2</sup> )	1.8
$r_F, r_R$ (m)	0.3
$B$	7
$C$	1.6
$D$	1.0

**Table 2** Steady-state cornering conditions and associated torque and steering inputs

Case	$R^{ss}$ (m)	$V^{ss}$ (m/s)	$\beta^{ss}$ (deg)	$T_F^{ss}$ (Nm)	$T_R^{ss}$ (Nm)	$\delta^{ss}$ (deg)	$\omega_F^{ss}$ (rad/s)	$\omega_R^{ss}$ (rad/s)	$\alpha_F^{ss}$ (deg)	$\alpha_R^{ss}$ (deg)
(a)	7	7	-10.4	-543	1194	3.2	22.27	32.08	-4.5	-22.5
(b)	7	7	-51	-56	1471	-40.7	20.44	58.33	-3.9	-57.9
(c)	7	6.12	-29	1649	-859	-13.7	21.13	2.9	-6.9	-39.1
(d)	7	7.41	-51	129	1456	-39.2	21.8	56.35	-5.4	-57.9
(e)	15	8.65	-33	1546	-902	-21.5	30.66	1.49	-7.8	-37.8
(f)	15	9.45	-29	-619	1375	-22.42	29.54	54.91	-2.9	-34
(g)	15	10.95	-51	38	1469	-42.53	34.25	75.45	-5.7	-54.5
(h)	1.5	3.42	-19	2031	-181	27.78	13.38	8.59	-4.4	-55.7
(i)	1.5	2.52	-37	-83	1376	11.36	6.76	38.37	-2	-64.3
(j)	1.5	3.42	-43	1267	1258	8.27	8.91	32.8	-4.2	-67.2
(k)	7	4	-6	-1395	1481	1.88	12.54	29.31	1.2	-18.4
(l)	7	5	-6	-1332	1478	1.1	15.69	29.36	2	-18.4
(m)	7	7	-6	-844	1213	-1.56	22.21	30.66	4.6	-18.4
(n)	7	4	-44	-845	1432	-37	11.56	69.35	0.2	-52
(o)	7	5	-44	-687	1450	-36	14.54	60.38	-0.7	-52
(p)	7	7	-44	-98	1400	-33	20.74	50.12	-3.9	-52

steady-states require both front and rear powered wheels (AWD) with appropriate torque distribution. On the other hand for the steady-state conditions (a), (b), (f), (i), (k)–(p) the input torques satisfy  $T_F^{ss} < 0$  and  $T_R^{ss} > 0$ , which are not achievable by a FWD vehicle. Finally, in Cases (c), (e) and (h) we observe that  $T_F^{ss} > 0$  and  $T_R^{ss} < 0$ , which are not achievable by a RWD vehicle. The latter steady-states require front powered wheel (FWD or AWD) and rear braking torque, for instance by application of the handbrake, similar to expert race driving techniques. This classification of the steady-state equilibria according to the require wheel torques will be considered rigorously in future extensions of this work.

Traditional stability analysis techniques using the understeering gradient (Gillespie, 1992), assume high values of the corner radius  $R^{ss}$ , small values of sideslip  $\beta^{ss}$  and operation of the tyres within their linear region. Hence, such techniques are not applicable to the operating regimes described in Table 2. For the given set of Magic Formula parameters in Table 1 it can be found that the maximum cornering tyre force (assuming free rolling of the tyre) is achieved at a slip angle

of 11.9 deg. We notice that for all the cases of steady-state conditions listed, the rear tyre has exceeded the saturation limit, operating well within the nonlinear region, as opposed to the front tyre, which suggests oversteering behaviour of the vehicle. In conditions (k), (l), (m), corresponding to the same cornering radius and slip angle, we observe that increasing steady-state velocity requires reduction of the steering angle (oversteering behaviour). On the other hand, in conditions (n), (o), (p), corresponding to the same cornering radius and a common high value of sideslip, we have the opposite effect, that is, increasing speed requires an increase in the steering angle. However, we notice that in the cases (n), (o), (p), the high sideslip angle steady-states are achieved with steering angle opposite to the direction of the corner (counter-steering). The decrease of the amount of counter-steering with the increase in velocity at high sideslip angles has been noted in Edelman et al. (2008) for a steady-state cornering condition referred to as power-slide. While traditional stability analysis, such as in Gillespie (1992), is not applicable in the operating regimes studied in this work, stability analysis of drifting steady-state cornering conditions using phase-plane techniques appears in Ono et al. (1998) and Hindiyeh and Gerdes (2009), or via root-locus in Edelman et al. (2008).

#### 4 Stabilisation of cornering equilibria

In the following, we present a control scheme to stabilise the vehicle with respect to the previously derived steady-state conditions. The proposed control architecture consists of an LQR controller which provides the necessary front and rear wheel longitudinal slips (slip ratios)  $s_{Fx}$  and  $s_{Rx}$  to stabilise the vehicle to a specified steady-state triplet  $(R^{ss}, V^{ss}, \beta^{ss})$ . A sliding mode controller uses individual front and rear wheel torque inputs to drive the front and rear wheel longitudinal slips to the values specified by the LQR controller. We consider the steering angle  $\delta$  as a parameter fixed to its steady-state value as calculated above, and we demonstrate stabilisation of the system using purely longitudinal control. Vehicle handling using longitudinal control is used by expert rally drivers, who regulate throttle and brake inputs to stabilise a vehicle during cornering, by taking advantage of the longitudinal load transfer during acceleration and deceleration (Velenis et al., 2007a, 2007b, 2008a, 2008b).

##### 4.1 Cornering control using longitudinal slip inputs

We first express the equations of motion of the single-track model equations (1)–(3) in terms of the state variables  $V$ ,  $\beta$  and  $\dot{\psi}$ :

$$\begin{aligned} \frac{d}{dt}V &= f_1(V, \beta, \dot{\psi}, s_{Fx}, s_{Rx}) \\ &= \frac{1}{m} [f_{Fx} \cos(\delta - \beta) - f_{Fy} \sin(\delta - \beta) + f_{Rx} \cos \beta + f_{Ry} \sin \beta], \end{aligned} \quad (27)$$

$$\begin{aligned} \frac{d}{dt}\beta &= f_2(V, \beta, \dot{\psi}, s_{Fx}, s_{Rx}) \\ &= \frac{1}{mV} [f_{Fx} \sin(\delta - \beta) + f_{Fy} \cos(\delta - \beta) - f_{Rx} \sin \beta + f_{Ry} \cos \beta - mV\dot{\psi}], \end{aligned} \quad (28)$$

$$\begin{aligned}\frac{d}{dt}\dot{\psi} &= f_3(V, \beta, \dot{\psi}, s_{Fx}, s_{Rx}) \\ &= \frac{\ell_F}{I_z} [f_{Fy} \cos \delta + f_{Fx} \sin \delta] - \frac{\ell_R}{I_z} f_{Ry}.\end{aligned}\quad (29)$$

The steady-state triplet  $(R^{ss}, V^{ss}, \beta^{ss})$  results in the equilibrium point  $(V^{ss}, \beta^{ss}, \dot{\psi}^{ss} = V^{ss}/R^{ss})$  of the above equations, that is

$$f_i(V^{ss}, \beta^{ss}, \dot{\psi}^{ss}, s_{Fx}^{ss}, s_{Rx}^{ss}) = 0, \quad i = 1, 2, 3,$$

where  $s_{ix}^{ss}$  ( $i = F, R$ ) are the steady-state front and rear wheel longitudinal slips, as calculated in Sections 3.1 and 3.2.

Equations (27)–(29) can be linearised as follows

$$\frac{d}{dt}\tilde{x} = \mathcal{A}^{ss}\tilde{x} + \mathcal{B}^{ss}\tilde{u}, \quad (30)$$

where  $\mathcal{A}^{ss}$  and  $\mathcal{B}^{ss}$  are the Jacobian matrices (with respect to the vehicle's state and slip inputs), computed at the equilibrium point  $(V^{ss}, \beta^{ss}, \dot{\psi}^{ss})$ , and

$$\tilde{x} = \begin{bmatrix} V - V^{ss} \\ \beta - \beta^{ss} \\ \dot{\psi} - \dot{\psi}^{ss} \end{bmatrix}, \quad \tilde{u} = \begin{bmatrix} s_{Fx} - s_{Fx}^{ss} \\ s_{Rx} - s_{Rx}^{ss} \end{bmatrix}, \quad \mathcal{C} = \mathcal{I}^{3 \times 3}.$$

The eigenvalues of  $\mathcal{A}^{ss}$ , which determine the stability of the equilibria are denoted by  $e_i$ ,  $i = 1, 2, 3$ . An LQR state feedback control law  $\tilde{u} = -\mathcal{K}\tilde{x}$  can then be readily computed using standard methods.

#### 4.2 Stabilisation of steady-state cornering via sliding-mode control

In this section we design a sliding-mode control scheme to stabilise the vehicle with respect to steady-state equilibria incorporating the wheel angular rate dynamics, and using independent front and rear wheel torque control.

Consider the systems (27)–(29) complemented by the dynamics of the rotating front and rear wheels equation (26). Recall that for a given operating condition of the vehicle  $(V, \beta, \dot{\psi})$ , a reference pair of front and rear longitudinal slip quantities  $s_{Fx}$  and  $s_{Rx}$  correspond to reference front and rear wheel speeds  $\omega_F$  and  $\omega_R$ , as in equations (24) and (25), respectively.

We define the variable  $\tilde{z}_i$  as the difference between the actual wheel angular rate  $\omega_i$  and a reference wheel angular rate corresponding to a reference value of longitudinal slip  $s_{ix}$ :

$$\tilde{z}_i = \omega_i - \phi_i(V, \beta, \dot{\psi}), \quad i = F, R,$$

where

$$\phi_i(V, \beta, \dot{\psi}) = \frac{V_{ix}}{(1 + s_{ix})r}, \quad i = F, R.$$

The reference slip quantities  $s_{ix}$  in the expression above are generated by the LQR stabilising control law.

Equation (31) results in

$$\begin{aligned} \dot{\tilde{z}}_i = & \frac{1}{I_w} T_i - \frac{r}{I_w} f_{ix} - \frac{\partial \phi_i}{\partial V}(V, \beta, \dot{\psi}) f_1(V, \beta, \dot{\psi}) \\ & - \frac{\partial \phi_i}{\partial \beta}(V, \beta, \dot{\psi}) f_2(V, \beta, \dot{\psi}) - \frac{\partial \phi_i}{\partial \dot{\psi}}(V, \beta, \dot{\psi}) f_3(V, \beta, \dot{\psi}). \end{aligned} \quad (31)$$

Consider the control input

$$T_i = T_i^{\text{eq}} + I_w \hat{v}_i, \quad (32)$$

where

$$T_i^{\text{eq}} = f_{ix} r + I_w \left( \frac{\partial \phi_i}{\partial V} f_1 + \frac{\partial \phi_i}{\partial \beta} f_2 + \frac{\partial \phi_i}{\partial \dot{\psi}} f_3 \right), \quad i = F, R. \quad (33)$$

The control component  $T_i^{\text{eq}}$  is referred to as the *equivalent control*. Taking  $T_i = T_i^{\text{eq}}$  results in  $\dot{\tilde{z}}_i = 0$  and ensures that the vehicle's states will remain in the *sliding manifold*  $\tilde{z}_i = 0$ . Equations (31)–(33) yield

$$\dot{\tilde{z}}_i = \hat{v}_i, \quad i = F, R. \quad (34)$$

Finally, we take

$$\hat{v}_i = -\lambda_i \text{sat}(\tilde{z}_i), \quad \lambda_i > 0, \quad i = F, R, \quad (35)$$

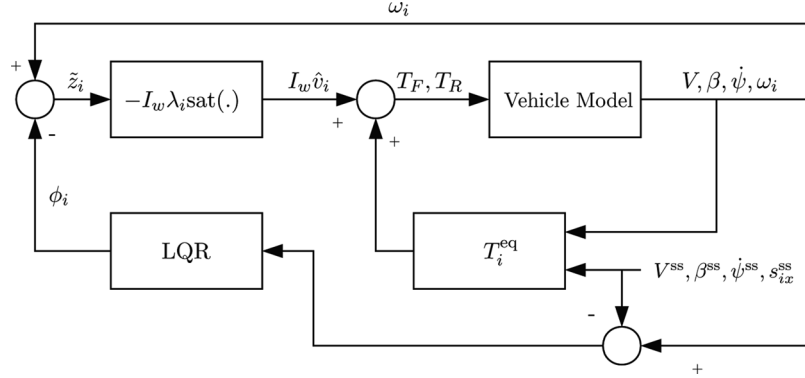
with

$$\text{sat}(\tilde{z}_i) = \begin{cases} \tilde{z}_i, & \text{if } |\tilde{z}_i| \leq 1, \\ \text{sign}(\tilde{z}_i), & \text{if } |\tilde{z}_i| > 1. \end{cases}$$

It can be readily shown that the control (35) stabilises equation (34) (Khalil, 1996). In fact, all trajectories starting off the *sliding manifold*  $\tilde{z}_i = 0$  will reach it in finite time under the control input (32). A schematic of the proposed control architecture is shown in Figure 2.

### 4.3 Stabilisation of cornering equilibria: numerical examples

We consider two simulation scenarios corresponding to Cases I and II of Table 3, where the stabilising control law of the previous section is implemented. Both cases correspond to unstable equilibria along the same path radius, negotiated at the same speed. Case I is a steady-state condition of moderate vehicle slip angle, while Case II is one of excessive slip angle. With these scenarios we demonstrate the ability of the control scheme to stabilise a variety of equilibria, including aggressive cases (Case II), which resemble vehicle operating regimes met by expert rally-race drivers (Velenis et al., 2007a, 2007b, 2008a, 2008b).

**Figure 2** Sliding mode control architecture for the stabilisation of steady-state cornering conditions**Table 3** Steady-state cornering equilibria

	Case I	Case II
$R^{ss}$ (m)	7	7
$V^{ss}$ (m/sec)	7	7
$\beta^{ss}$ (deg)	-10.4	-51
$s_{Rx}^{ss}$	-0.2871	-0.7491
$s_{Fx}^{ss}$	0.0244	0.0026
$\delta^{ss}$ (deg)	3.2	-40.7
$e_1$	$0.7484 + 1.1395i$	$0.5790 + 0.7196i$
$e_2$	$0.7484 - 1.1395i$	$0.5790 - 0.7196i$
$e_3$	-9.9095	-8.8562

The parameters of the vehicle model are shown in Table 1. In Case I, the simulation starts with initial states perturbed as follows,

$$V(0) = 1.2 \times V^{ss}, \quad \beta(0) = 2 \times \beta^{ss}, \quad \dot{\psi}(0) = 1.2 \times \dot{\psi}^{ss}, \quad (36)$$

whereas in Case II the simulation starts from the following initial conditions:

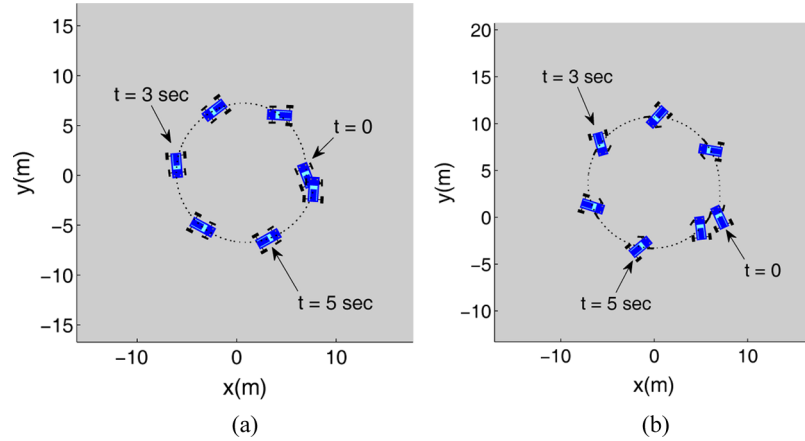
$$V(0) = 1.2 \times V^{ss}, \quad \beta(0) = \beta^{ss}/2, \quad \dot{\psi}(0) = 1.2 \times \dot{\psi}^{ss}. \quad (37)$$

In addition, we consider initial wheel speeds  $\omega_F(0)$  and  $\omega_R(0)$ , such that the initial longitudinal slip at the front and rear wheels are both zero (free rolling wheels). The controller (32) is implemented in both cases with  $\lambda_i = 100 \text{ sec}^{-1}$  ( $i = F, R$ ).

The resulting trajectories for the two simulation scenarios are shown in Figure 3. The vehicle states, torque control inputs and longitudinal wheel slips for the simulation Cases I and II are shown in Figures 4 and 5, respectively. In the velocity  $V$ , sideslip angle  $\beta$ , yaw rate  $d\psi/dt$  and longitudinal slips  $s_{ix}$  plots we present, in addition, the response of the vehicle model under the action of the LQR controller of Section 4.1 (dotted curves) assuming longitudinal slip control inputs during stabilisation from the same initial conditions. The wheel angular rates  $\omega_F$  and  $\omega_R$  corresponding to the response of the model under longitudinal slip inputs

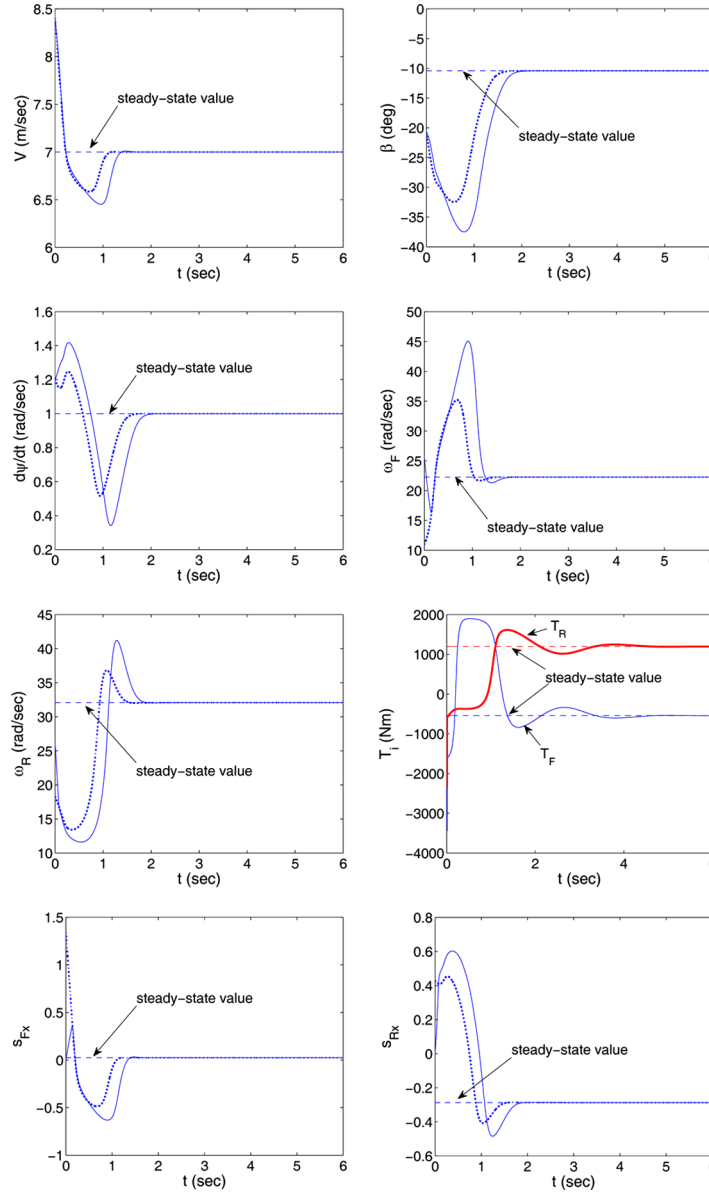
(dotted  $\omega_F$  and  $\omega_R$  curves) were calculated using equations (24) and (25), where  $s_{F_x}$  and  $s_{R_x}$  were the control inputs of the LQR controller. Hence, the dotted  $\omega_i$  response curves correspond to the sliding manifold which is successfully met by the sliding mode controller  $T_i$  in finite time, in both Cases I and II.

**Figure 3** Steady-state cornering stabilisation via sliding mode control; simulation scenarios from Section 4.3: (a) Case I and (b) Case II (see online version for colours)



In the design of the control scheme to stabilise the vehicle with respect to the steady-state cornering equilibria we have assumed exact knowledge of the tyre/road friction forces via Pacejka's Magic Formula. In reality, such information is rarely accurately available due to the number of parameters that affect the tyre-road interaction forces. To this end, we simulate the performance of the stabilising controller in the presence of uncertainty in the tyre friction. In particular, we assume uncertainty in the parameter  $D$  of the Magic Formula (6), which coincides with the maximum value of the friction coefficient for a given road condition. Typically  $D = 0.9 - 1$  corresponds to dry asphalt surface,  $D = 0.7 - 0.8$  corresponds to wet asphalt,  $D = 0.5 - 0.6$  to gravel, and  $D = 0.2$  to ice. In Figure 6 we present the vehicle response and torque control inputs during stabilisation of the steady-state condition of Case II, where the controller is designed using a nominal value of  $D = 1$ , and tested in three different actual values of  $D$ , namely,  $D = 1$ ,  $D = 0.75$  and  $D = 0.5$ . We observe that the controller is successful in stabilising the vehicle at a steady-state cornering condition. In the presence of uncertainty in the tyre friction coefficient (cases of  $D = 0.75$ ,  $D = 0.5$ ) we notice a steady-state error in all of the vehicle states, and the error increases with the increase in the deviation of the friction coefficient. In particular, we observe that the vehicle is stabilised at a lower velocity and lower yaw rate than the initial steady-state condition of Case II, which is the result of the decrease in the friction coefficient and hence the maximum available cornering acceleration. We conclude that the control scheme introduces a level of robustness with respect to the tyre friction uncertainty, however, in order to avoid significant steady-state errors in the vehicle response, actual implementation of the controller will require real time tyre friction estimation as demonstrated, for instance, in Hsu and Gerdes (2005) and Piyabongkarn et al. (2009).

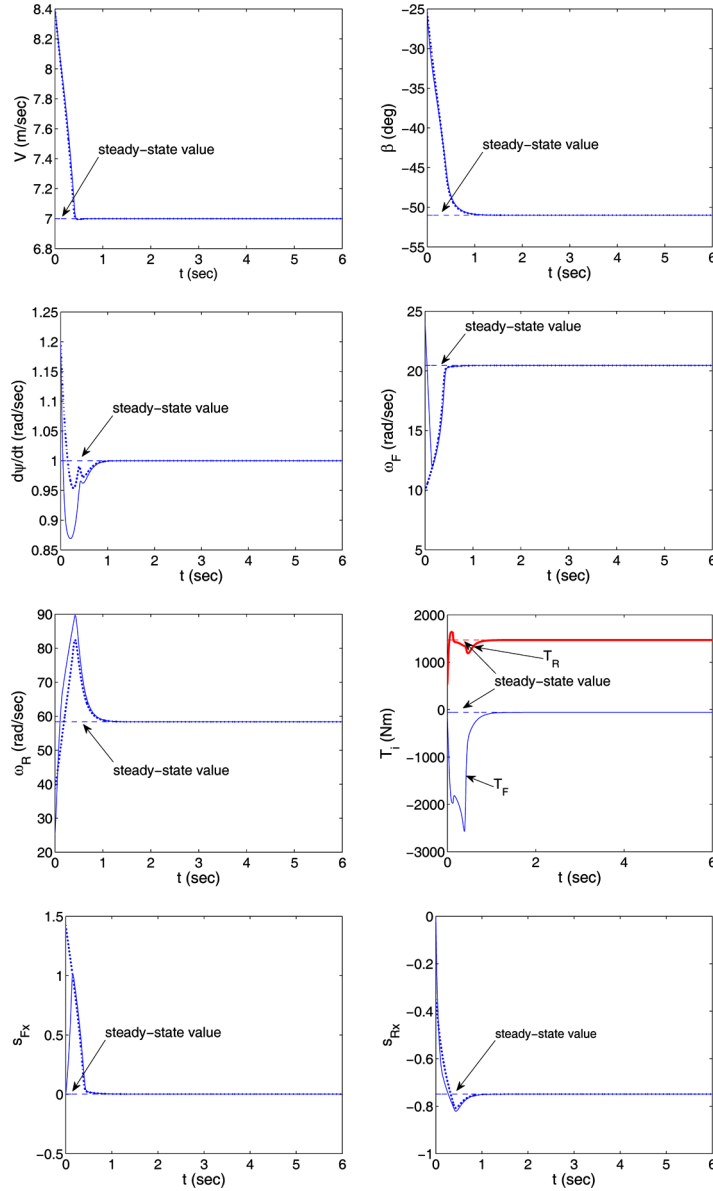
**Figure 4** Case I: Vehicle states, torque control inputs and longitudinal wheel slips. The dotted curves correspond to the stabilisation of the vehicle model using longitudinal slip control inputs (see online version for colours)



#### 4.4 Incorporating suspension dynamics

In this section we implement the sliding mode controller using a vehicle model of increased fidelity. In particular, we introduce a single-track model with suspension dynamics, and demonstrate the performance of the controller in the same simulation scenarios as in the previous section.

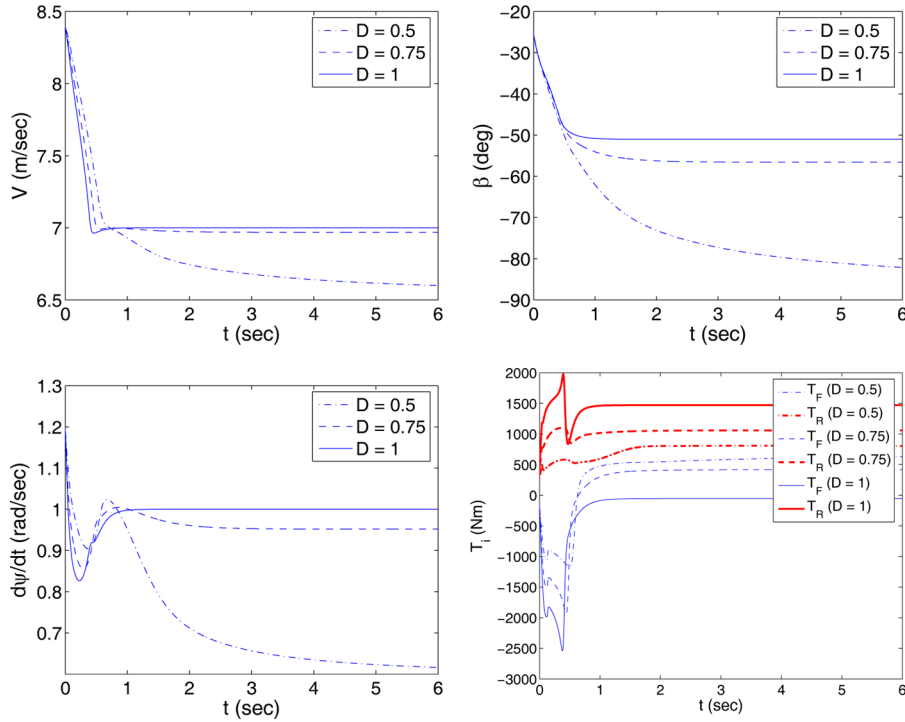
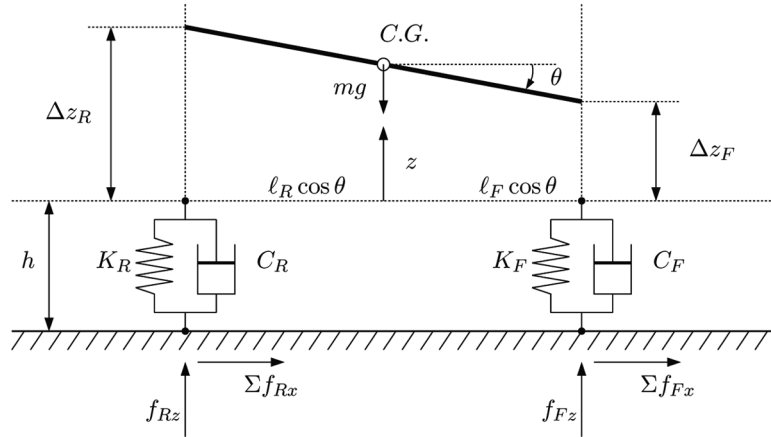
**Figure 5** Case II: Vehicle states, torque control inputs and longitudinal wheel slips. The dotted curves correspond to the stabilisation of the vehicle model using longitudinal slip control inputs (see online version for colours)



Let  $z$  be the vertical displacement of the centre of gravity of the vehicle and  $\theta$  the pitch angle of the suspended mass as in Figure 7. The dynamics of the vertical translation and pitch rotation motions of the suspended mass are described by the following equations

$$m\ddot{z} = f_{Fz} + f_{Rz} - mg, \tag{38}$$

$$I_y\ddot{\theta} = f_{Rz}\ell_R \cos \theta - f_{Fz}\ell_F \cos \theta - \Sigma f_{Rx}(h + z) - \Sigma f_{Fx}(h + z), \tag{39}$$

**Figure 6** Case II: Vehicle states and torque control inputs in the presence of tyre friction uncertainty (see online version for colours)

**Figure 7** Suspension dynamics


where  $I_y$  is the moment of inertia of the vehicle about the  $y$  body axis,  $h$  is the vertical distance of the CG from the ground in an equilibrium state with  $z = 0$ , and  $\Sigma f_{ix}$  ( $i = F, R$ ) is the projection of the total friction force of each wheel on the  $x$  body axis. Furthermore,

$$\Sigma f_{Rx} = f_{Rx} \quad \text{and} \quad \Sigma f_{Fx} = f_{Fx} \cos \delta - f_{Fy} \sin \delta.$$

Given the vertical displacement of the CG  $z$ , and the pitch angle  $\theta$ , the normal load of each wheel is given by

$$\begin{aligned} f_{Fz} &= f_{Fz}^o - K_F \Delta z_F - C_F \Delta \dot{z}_F \\ f_{Rz} &= f_{Rz}^o - K_R \Delta z_R - C_R \Delta \dot{z}_R \end{aligned}$$

where

$$\begin{aligned} \Delta z_R &= z + \ell_R \sin \theta, & \Delta z_F &= z - \ell_F \sin \theta \\ \Delta \dot{z}_R &= \dot{z} + \dot{\theta} \ell_R \cos \theta, & \Delta \dot{z}_F &= \dot{z} - \dot{\theta} \ell_F \cos \theta \end{aligned}$$

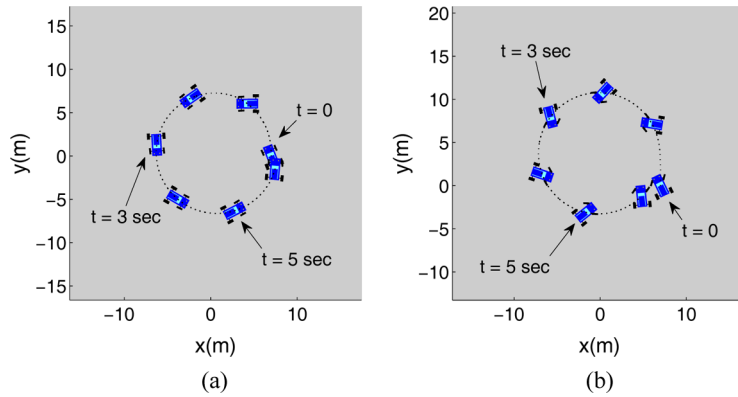
and

$$f_{Fz}^o = mg \frac{\ell_R}{\ell_F + \ell_R}, \quad f_{Rz}^o = mg \frac{\ell_F}{\ell_F + \ell_R}.$$

Next, we present simulation results of the implementation of the sliding mode control law of Section 4.2 using the single-track model with suspension dynamics (27)–(29), (26), (38) and (39). The parameters of the vehicle model used are shown in Table 1. In addition, we use  $K_F = K_R = 10,000 \text{ N/m}$ ,  $C_F = C_R = 2000 \text{ Nsec/m}$  and  $I_y = 2741.9 \text{ kgm}^2$ .

We consider two simulation scenarios of stabilising the vehicle with respect to the equilibrium Cases I and II as in Table 3. The initial conditions in Cases I and II are given by equations (36) and (37) respectively. In addition, we consider initial wheel speeds  $\omega_F(0)$  and  $\omega_R(0)$  such that the initial longitudinal slip at the front and rear wheels are both zero, i.e., we enforce initial free rolling of the front and rear wheels. Finally, we assume zero initial vertical displacement and velocity and zero pitch angle and pitch rate ( $z(0) = \dot{z}(0) = 0$ ,  $\theta(0) = \dot{\theta}(0) = 0$ ). The controller (32) is implemented in both cases with  $\lambda_i = 100 \text{ sec}^{-1}$  ( $i = F, R$ ). The resulting trajectories for the two simulation scenarios are shown in Figure 8. The vehicle states, including the suspension dynamics states, and control inputs for the simulation

**Figure 8** Steady-state cornering stabilisation of a single-track model with suspension dynamics; Steady-state equilibrium points from Table 3 (a) Case I and (b) Case II (see online version for colours)



Cases I and II are shown in Figures 9 and 10 respectively. The wheel torque control inputs and vehicle states corresponding to the sliding mode stabilisation of the single-track model (27)–(29), equation (26) incorporating the static map of longitudinal acceleration to normal load transfer (9), (10) (neglecting the suspension dynamics) are also presented in Figures 9 and 10 (dotted curves) for comparison. The sliding mode controller successfully stabilises the higher order vehicle model including suspension dynamics, despite the fact that the steady-state cornering conditions were derived using the lower order vehicle model.

**Figure 9** Vehicle states and torque control inputs during stabilisation of steady-state equilibrium point Case I. The dotted curves correspond to the stabilisation of the vehicle model neglecting the suspension dynamics (see online version for colours)

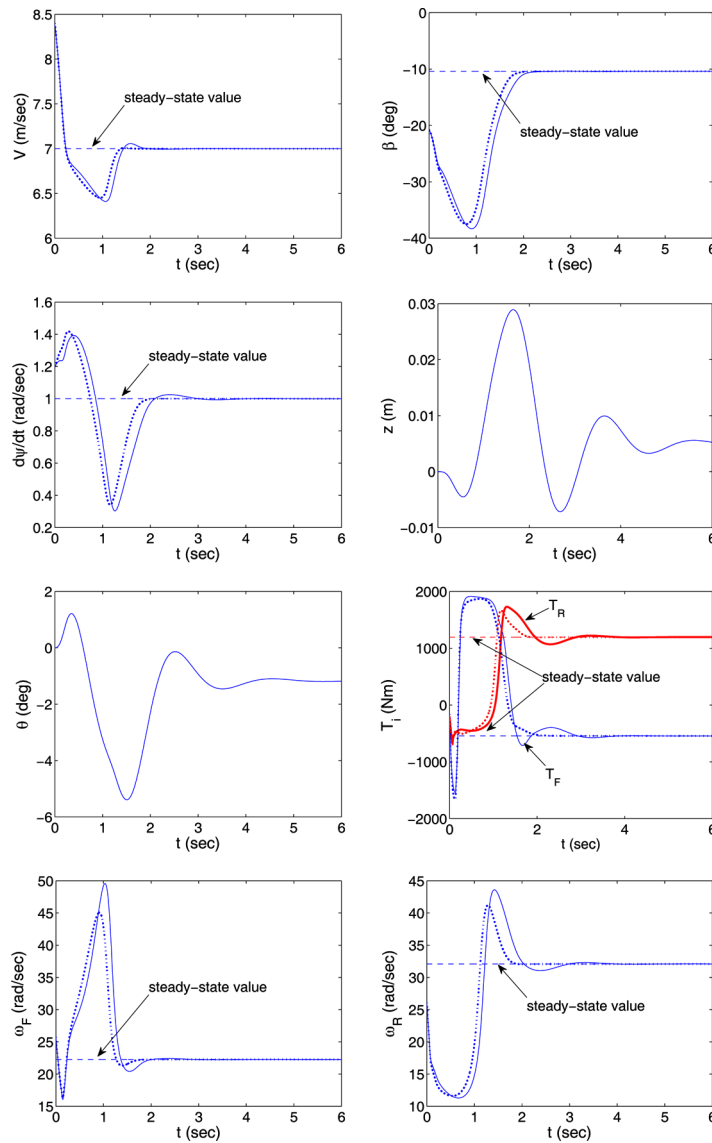
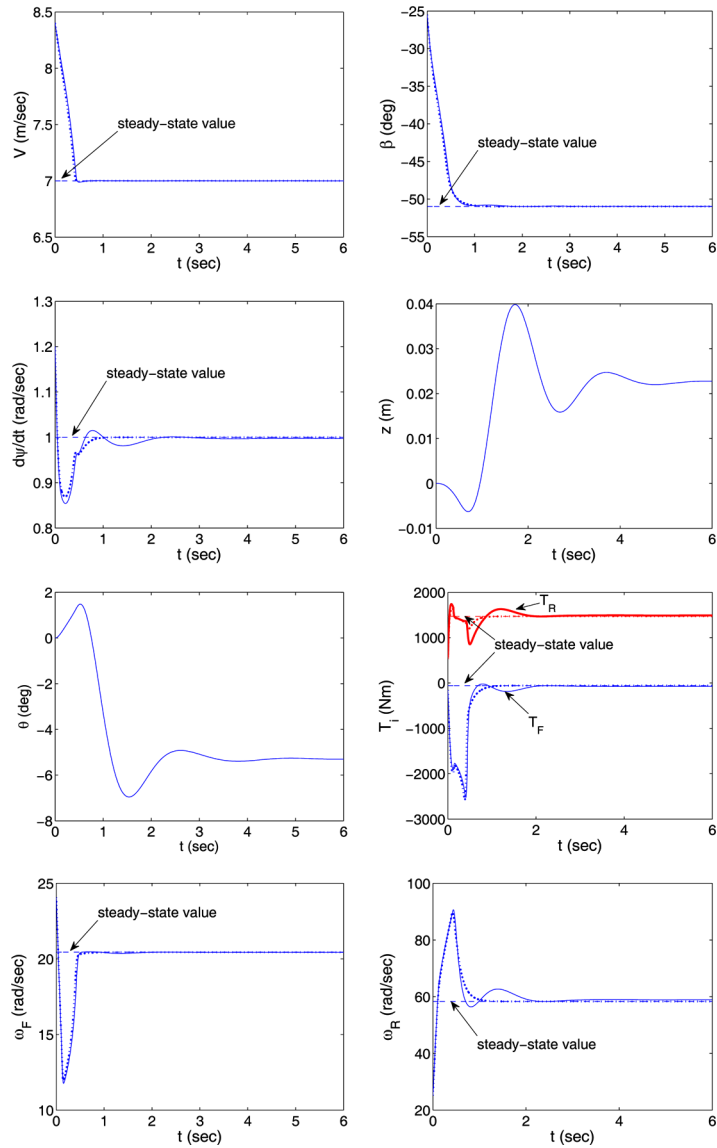


**Figure 10** Vehicle states and torque control inputs during stabilisation of steady-state equilibrium point Case II. The dotted curves correspond to the stabilisation of the vehicle model neglecting the suspension dynamics (see online version for colours)



## 5 Conclusions

In this work we studied the control of wheeled vehicles in extreme operating conditions. We explicitly derived steady-state cornering conditions for a vehicle with the tyres operating in their nonlinear region. The resulting trajectories included cases of aggressive sideslip angle similar to driving techniques used by expert rally drivers. Motivated by recently studied race driving techniques, we demonstrated

that stabilisation of these extreme steady-states may be achieved using longitudinal (accelerating/braking) control. In particular, we designed a sliding mode controller using front and rear wheel torque inputs to stabilise the vehicle dynamics with respect to the above steady-state cornering conditions. The controller's performance was validated by increasing the level of detail of the initial vehicle model to include suspension dynamics.

Plans for future work include the extension of the current results using vehicle models of increasing fidelity (e.g., four wheel models incorporating lateral load transfer effects) and implementation of the control scheme on an autonomous vehicle platform.

### Acknowledgements

The work of the first author was supported by a Marie Curie International Reintegration Grant within the 7th European Community Framework Programme and a Brunel University BRIEF Award. The work of the second author was supported by ARO Award W911NF-07-1-0499. The work of the third author was supported by ARO Award No. W911NF-05-1-0331 and NSF GOALI Award No. CMMI-0727768.

### References

- Abdulrahim, M. (2006) 'On the dynamics of automobile drifting', *SAE World Congress*, 3–6 April, Detroit, MI, pp.169–178.
- Ackermann, J. (1997) 'Robust control prevents car skidding', *IEEE Control Systems Magazine*, Vol. 17, pp.23–31.
- Bakker, E., Nyborg, L. and Pacejka, H.B. (1987) 'Tyre modelling for use in vehicle dynamics studies', *SAE International Congress and Exposition*, Detroit, MI, SAE Paper No. 870421.
- Dang, N.J. (2004) *Preliminary Results Analysing the Effectiveness of Electronic Stability Control ESC Systems*, National Highway Traffic Safety Administration, Washington DC, September, DOT HS 809 790.
- Edelmann, J., Plöchl, M., Lugner, P., Mack, W. and Falkner, A. (2008) 'Investigations on the powerslide of automobiles', *9th International Symposium of Advanced Vehicle Control (AVEC)*, 6–9 October, Kobe, Japan.
- Frazzoli, E. (2008) 'Discussion on "Optimality Properties and Driver Input Parameterization for Trail-Braking Cornering"', *European Journal of Control*, Vol. 14, No. 4, July–August, pp.321–324.
- Frazzoli, E., Dahleh, M.A. and Feron, E. (2002) 'Real-time motion planning for agile autonomous vehicles', *Journal of Guidance, Control and Dynamics*, Vol. 25, No. 1, pp.116–129.
- Frazzoli, E., Dahleh, M.A. and Feron, E. (2005) 'Maneuver-based motion planning for nonlinear systems with symmetries', *IEEE Transactions on Robotics*, Vol. 21, No. 6, pp.1077–1091.
- Gillespie, T.D. (1992) *Fundamentals of Vehicle Dynamics*, Society of Automotive Engineers SAE International, Warrendale, PA, USA.

- Hac, A. and Bodie, M.O. (2002) 'Improvements in vehicle handling through integrated control of chassis systems', *International Journal of Vehicle Design*, Vol. 29, Nos. 1–2, pp.23–50.
- Hindiyeh, R.Y. and Gerdes, J.C. (2009) 'Equilibrium analysis of drifting vehicles for control design', *Proceedings of the ASME 2009 Dynamic Systems and Control Conference*, 12–14 October, Hollywood, CA, USA, pp.181–188.
- Hsu, Y.H.J. and Gerdes, J.C. (2005) 'Stabilization of a steer-by-wire vehicle at the limits of handling using feedback linearization', *ASME International Mechanical Engineering Congress and Exposition*, 5–11 November, Orlando, FL, USA.
- Ikushima, Y. and Sawase, K. (1995) 'A study on the effects of the active yaw moment control', *SAE International Congress and Exposition*, 27 February–2 March, Detroit, MI, SAE Paper 950303.
- Khalil, H.K. (1996) *Nonlinear Systems*, 2nd ed., Prentice-Hall, Upper Saddle River, New Jersey.
- Kim, D., Hwang, S. and Kim, H. (2008) 'Vehicle stability enhancement of four-wheel-drive hybrid electric vehicle using rear motor control', *IEEE Transactions on Vehicular Technology*, Vol. 57, No. 2, March, pp.727–735.
- Ono, E., Hosoe, S., Tuan, H.D. and Doi, S. (1998) 'Bifurcation in vehicle dynamics and robust front wheel steering control', *IEEE Transactions on Control Systems Technology*, Vol. 6, No. 3, May, pp.412–420.
- Piyabongkarn, D., Lew, J.Y., Rajamani, R., Grogg, J.A. and Yuan, Q. (2007) 'On the use of torque biasing systems for electronic stability control: limitations and possibilities', *IEEE Transactions on Control Systems Technology*, Vol. 15, No. 3, May, pp.581–589.
- Piyabongkarn, D., Rajamani, R., Grogg, J.A. and Lew, J.Y. (2009) 'Development and experimental evaluation of a slip angle estimator for vehicle stability control', *IEEE Transactions on Control Systems Technology*, Vol. 17, No. 1, January, pp.78–88.
- van Zanten, A.T., Erhardt, R., Landesfeind, G. and Pfa, K. (2000) 'Vehicle stabilization by the vehicle dynamics control system ESP', *IFAC Mechatronic Systems*, Darmstadt, Germany, pp.95–102.
- Tahami, F., Kazemi, R. and Farhanghi, S. (2003) 'A novel driver assist stability system for all-wheel-drive electric vehicles', *IEEE Transactions on Vehicular Technology*, Vol. 52, No. 3, May, pp.683–692.
- Trachtler, A. (2004) 'Integrated vehicle dynamics control using active brake steering and suspension systems', *International Journal of Vehicle Design*, Vol. 36, No. 1, pp.1–12.
- Velenis, E., Tsiotras, P. and Lu, J. (2007a) 'Modeling aggressive maneuvers on loose surfaces: the cases of trail-braking and pendulum-turn', *Proceedings of the 2007 European Control Conference*, 2–5 July, Kos, Greece, pp.1233–1240.
- Velenis, E., Tsiotras, P. and Lu, J. (2007b) 'Aggressive maneuvers on loose surfaces: data analysis and input parameterization', *Proceedings of the 2007 Mediterranean Conference on Control and Automation*, 27–29 June, Athens, Greece, pp.1–6.
- Velenis, E., Tsiotras, P. and Lu, J. (2008a) 'Trail-braking driver input parameterization for general corner geometry', *Proceedings of the SAE Motorsports Engineering Conference*, 2–4 December, Concord, NC, USA, SAE Paper 2008-1-2986.
- Velenis, E., Tsiotras, P. and Lu, J. (2008b) 'Optimality properties and driver input parameterization for trail-braking cornering', *European Journal of Control*, Vol. 14, No. 4, July–August, pp.308–320.
- Wei, J., Zhuoping, Y. and Lijun, Z. (2006) 'Integrated chassis control system for improving vehicle stability', *Proceedings of the IEEE International Conference on Vehicular Electronics and Safety*, 6–9 December, Shanghai, China, pp.295–298.

- Yi, J. and Tseng, E.H. (2009) 'Nonlinear stability analysis of vehicle lateral motion with a hybrid physical/dynamic tyre/road friction model', *Proceedings of the ASME 2009 Dynamic Systems and Control Conference*, 12–14 October, Hollywood, CA, USA, pp.509–516.
- Yoshimoto, K., Tanaka, H. and Kawakami, S. (1999) 'Proposal of driver assistance system for recovering vehicle stability from unstable states by automatic steering', *Proceedings of the IEEE International Vehicle Electronics Conference*, 6–9 September, Changchun, China, pp.514–519.